Oxidation of methane by a biological dicopper centre

Ramakrishnan Balasubramanian[1,2]*, Stephen M. Smith[1,2]*, Swati Rawat[3], Liliya A. Yatsunyk[1,2], Timothy L. Stemmler[3] & Amy C. Rosenzweig[1,2]

Vast world reserves of methane gas are underutilized as a feedstock for the production of liquid fuels and chemicals owing to the lack of economical and sustainable strategies for the selective oxidation of methane to methanol[1]. Current processes to activate the strong C–H bond (104 kcal mol^{-1}) in methane require high temperatures, are costly and inefficient, and produce waste[2]. In nature, methanotrophic bacteria perform this reaction under ambient conditions using metalloenzymes called methane monooxygenases (MMOs). MMOs thus provide the optimal model for an efficient, environmentally sound catalyst[3]. There are two types of MMO. Soluble MMO (sMMO) is expressed by several strains of methanotroph under copper-limited conditions and oxidizes methane with a well-characterized catalytic di-iron centre[4]. Particulate MMO (pMMO) is an integral membrane metalloenzyme produced by all methanotrophs and is composed of three subunits, pmoA, pmoB and pmoC, arranged in a trimeric α$_3$β$_3$γ$_3$ complex[5]. Despite 20 years of research and the availability of two crystal structures, the metal composition and location of the pMMO metal active site are not known. Here we show that pMMO activity is dependent on copper, not iron, and that the copper active site is located in the soluble domains of the pmoB subunit rather than within the membrane. Recombinant soluble fragments of pmoB (spmoB) bind copper and have propylene and methane oxidation activities. Disruption of each copper centre in spmoB by mutagenesis indicates that the active site is a dicopper centre. These findings help resolve the pMMO controversy and provide a promising new approach to developing environmentally friendly C–H oxidation catalysts.

Three distinct metal centres were identified in the 2.8 Å-resolution structure of pMMO from *Methylococcus capsulatus* (Bath)[6,7] (Fig. 1). Two copper centres are located in the soluble regions of the pmoB subunit, which form two cupredoxin domains. A dicopper centre with a short Cu–Cu distance of 2.5–2.7 Å (refs 8, 9) is coordinated by the highly conserved[5] residues His 33, His 137 and His 139 and is also observed in pMMO from *Methylosinus trichosporium* OB3b[10]. The second site, a monocopper centre coordinated by His 48 and His 72, is not conserved in pMMO from *M. trichosporium* OB3b. A third metal centre, occupied by zinc from the crystallization buffer, is located within the membrane and is ligated by Asp 156, His 160 and His 173 from pmoC and possibly Glu 195 from pmoA (ref. 6). This site contains a copper ion in the structure of *M. trichosporium* OB3b pMMO[10].

The nature of the pMMO metal active site is not established and has been intensely controversial[11,12]. On the basis of electron paramagnetic resonance spectroscopic data, pMMO was initially proposed to contain multiple trinuclear copper clusters[13,14]. In light of the crystallographic data, this model was revised to a single catalytic tricopper cluster located at an intramembrane site composed of conserved hydrophilic residues[15] (Fig. 1). This model also includes the

binding of an additional ten copper ions to the C-terminal soluble domain of pmoB (ref. 16). Both this intramembrane site and the C-terminal domain of pmoB are devoid of metal ions in the crystal
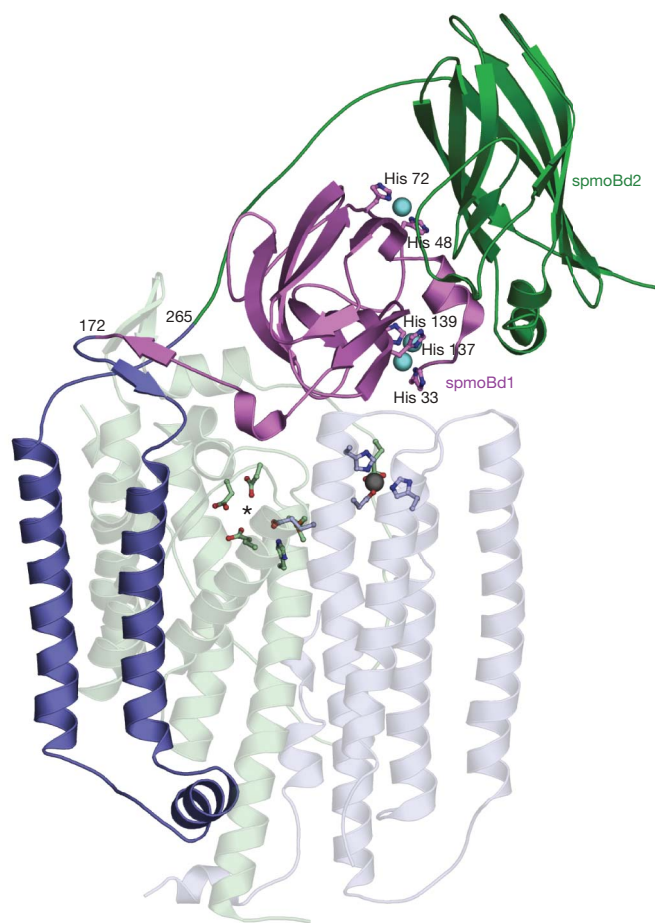

Figure 1 | Structure of the *M. capsulatus* (Bath) pMMO protomer. The amino-terminal cupredoxin domain of pmoB (spmoBd1) is shown in purple, the carboxy-terminal cupredoxin domain of pmoB (spmoBd2) is shown in green and the two transmembrane helices are shown in blue. In the recombinant spmoB protein, spmoBd1 and spmoBd2 are connected by a Gly-Lys-Leu-Gly-Gly-Gly sequence linking residues 172 and 265 (indicated), rather than the two transmembrane helices. Copper ions are shown as cyan spheres and ligands are shown as ball-and-stick representations. The pmoA (faint light green) and pmoC (faint light blue) subunits are composed of transmembrane helices. The location of the zinc ion (grey sphere) has been proposed to contain a di-iron centre. A hydrophilic patch of residues, marked with an asterisk, is the site of a proposed tricopper centre. Protein Data Bank ID, 1YEW.

[1]Department of Biochemistry, Molecular Biology and Cell Biology, [2]Department of Chemistry, Northwestern University, Evanston, Illinois 60208, USA. [3]Department of Biochemistry and Molecular Biology, Wayne State University, School of Medicine, Detroit, Michigan 48201, USA.
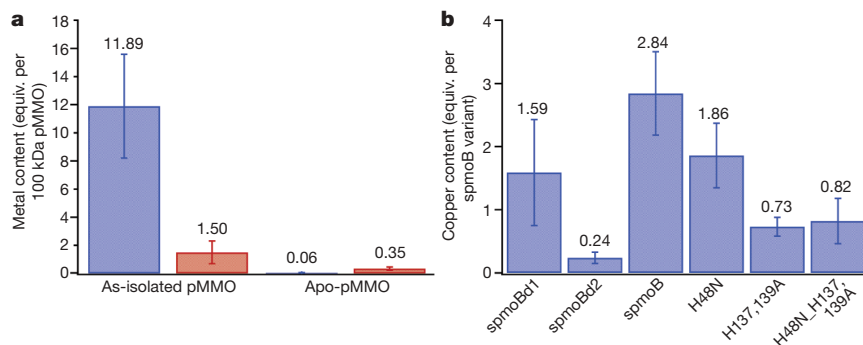*These authors contributed equally to this work.

Figure 2 | Metal analysis. a, Metal content of as-isolated pMMO and apo-pMMO prepared by cyanide treatment. Metal content is expressed per 100 kDa pMMO protomer, with copper in blue and iron in red. **b**, Copper content of refolded spmoB variants. Reported values and errors represent the average and standard deviation of at least four independent measurements for pMMO samples and at least six independent refolding experiments for each spmoB variant.

structures. By contrast, Mössbauer spectroscopic data led to the suggestion that the pMMO active site is a di-iron centre located at the intramembrane site occupied by zinc in the structure of *M. capsulatus* (Bath) pMMO (Fig. 1) and by copper in that of *M. trichosporium* OB3b pMMO (ref. 17).

To determine the metal requirement for pMMO activity, we first removed the metals from as-isolated *M. capsulatus* (Bath) pMMO membranes by treatment with cyanide (Fig. 2a). Before cyanide treatment, as-isolated samples had propylene epoxidation activities of 50–200 nmol propylene oxide mg^{-1} min^{-1}. These values are comparable to or higher than values reported by other researchers for as-isolated membranes[18–20] (Supplementary Table 1). We used membranes rather than purified pMMO to resemble the natural environment more closely and to avoid activity loss typically observed upon solubilization and purification[9]. Cyanide treatment completely abolished pMMO activity as measured by the propylene epoxidation assay.

We then titrated stoichiometric amounts of copper and/or iron into the apo pMMO samples and assessed the effects on activity. Addition of 2–3 equiv. of copper per 100 kDa pMMO protomer restored ~70% of the propylene epoxidation activity (Fig. 3a). We also tested the ability of pMMO reconstituted with copper to oxidize methane to methanol. As-isolated pMMO has a specific activity of 22.9 ± 6.1 nmol methanol mg^{-1} min^{-1}, and apo-pMMO reconstituted with 3 equiv. of copper had an activity of 21.7 ± 3.5 nmol methanol mg^{-1} min^{-1}, restoring greater than 90% of the methane oxidation activity (Fig. 3b). By contrast, addition of iron, aerobically or anaerobically, does not restore or improve activity if added alone or in combination with copper.

These experiments demonstrate that copper, not iron[17], is the metal at the active site of pMMO. The requirement for only 2–3 equiv. of copper indicates that large numbers of copper ions may not be necessary for activity, as proposed previously[12]. Some of the copper associated with the as-isolated membranes may instead be bound adventitiously. Notably, addition of copper beyond three equiv. inhibits pMMO activity. Repeating the cyanide treatment and adding back 2–3 equiv. of copper can reverse this inhibition (Supplementary Fig. 1a). The excess copper ions probably react with reductant to generate hydrogen peroxide, which reversibly inhibits pMMO. This phenomenon has been studied for pMMO from *M. trichosporium* OB3b[21]. In support of this explanation, catalase prevents inhibition on addition of excess copper, with maximal activity still observed at 2–3 equiv. (Supplementary Fig. 1b).

To probe the coordination environment of copper in pMMO, we collected X-ray absorption spectroscopic (XAS) data. As-isolated pMMO is a mixture of Cu(I) and Cu(II) as shown by both a $1s \rightarrow 4p$ transition and a weak $1s \rightarrow 3d$ feature[22] in the near-edge spectra (Supplementary Fig. 2). Apo-pMMO reconstituted with 3 equiv. of CuSO$_4$ and treated with duroquinol to mimic the activity assay conditions has a stronger Cu(I) $1s \rightarrow 4p$ transition consistent with the presence of reductant (Supplementary Fig. 2). Fourier transforms (Fig. 4b, d) of the extended X-ray absorption fine structure (EXAFS) data (Fig. 4a, c) for both samples show two scattering interactions corresponding to nearest-neighbour ligands at approximately 2 Å and 2.5 Å. Long-range ligand scattering (>3 Å) is also evident. The as-isolated pMMO EXAFS data were best fitted with two Cu–O/N environments at 1.92 Å and 2.09 Å and a Cu–Cu interaction centred at 2.66 Å. The reconstituted pMMO EXAFS data were best fitted with a single set of O/N ligands at 1.95 Å. Most important, there was a significant improvement in fit when a Cu–Cu scattering environment centred at 2.53 Å was included (Supplementary Table 2). Debye–Waller factors, which are measures of the metal–ligand bond disorder, were high in both Cu–Cu interaction simulations (>5.5 × 10^{-3} Å^2), whereas the coordination numbers were consistently low (≤0.25). These results indicate either a near-stoichiometric population of distinct, but non-resolvable, Cu–Cu interactions with destructively overlapping scattering centred at 2.66 Å and 2.53 Å or low populations (less than 25%) of bound copper coordinated in a multinuclear cluster. Regardless, restoration of activity on copper addition is accompanied by formation of a copper cluster, which is probably the dinuclear copper centre observed in the crystal structures[6,10].
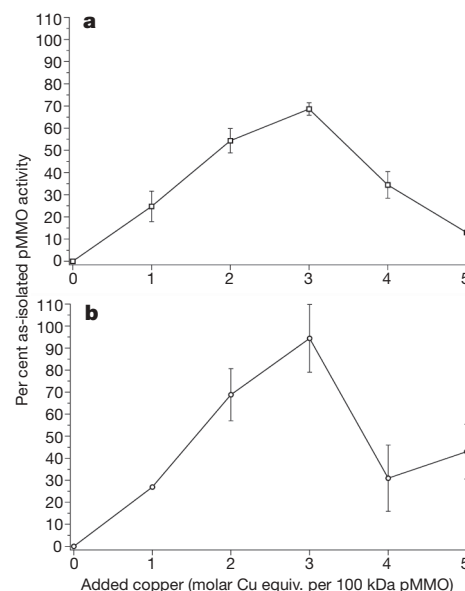

Figure 3 | Restoration of activity to apo-pMMO by the addition of copper. Copper equivalents added are expressed per 100 kDa pMMO protomer. Representative titrations are shown. Addition of 2–3 equiv. of copper restored ~70% of the propylene epoxidation activity (**a**) and ~90% of the methane oxidation activity (**b**). Reported values represent the average and standard deviation of at least two measurements.
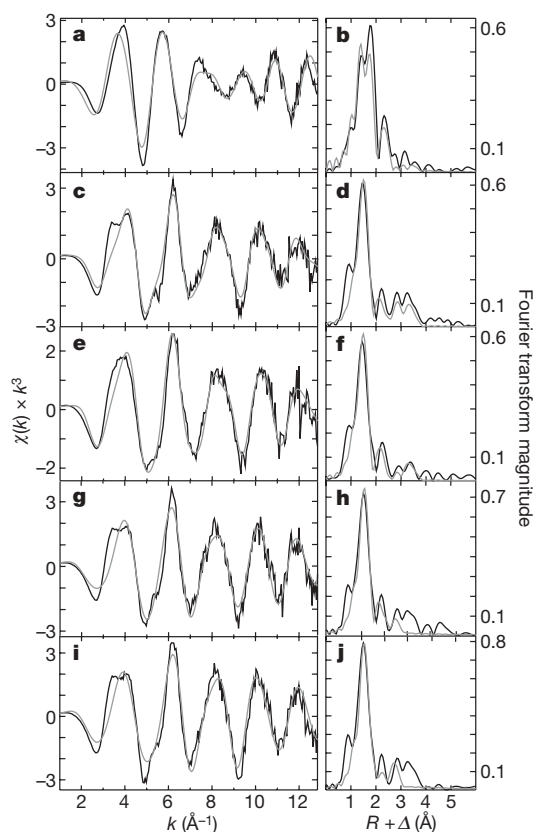
Figure 4 | Copper EXAFS data and simulations for pMMO and spmoB variants. Raw k^3-weighted EXAFS data and phase-shifted Fourier transforms are shown for as-isolated pMMO (**a**, **b**), copper reconstituted pMMO (**c**, **d**), spmoB (**e**, **f**), spmoB_H48N (**g**, **h**), and spmoB_H137,139A (**i**, **j**). Raw unfiltered data are shown in black and best-fit simulations are shown in grey. χ, EXAFS region of the XAS spectrum; Δ, apparent shift in Fourier transform displayed bond distance (by ~ -0.5 Å) due to a phase shift during calculation of the transform; k, photoelectron wavevector; R, metal–ligand bond length.

Possible locations for the active site in *M. capsulatus* (Bath) include the two copper centres in the soluble regions of pmoB, the intramembrane zinc site and the intramembrane hydrophilic patch proposed to contain a trinuclear copper site (Fig. 1)[11]. We cloned and expressed in *Escherichia coli* several proteins corresponding to the soluble cupredoxin domains of the pmoB subunit. These proteins include the amino (N)-terminal cupredoxin domain (spmoBd1, residues 33–172), the carboxy (C)-terminal cupredoxin domain (spmoBd2, residues 265–414) and both domains tethered by a Gly-Lys-Leu-Gly-Gly-Gly linker, which replaces the two transmembrane helices (spmoB) (Fig. 1). All ligands to the two copper centres are contained within spmoBd1, although the mononuclear site lies at the domain interface.

These recombinant proteins were refolded from solubilized inclusion bodies in the presence of $CuSO_4$. Copper analysis by the bicinchoninic-acid method[23] indicates the presence of 2.84 ± 0.66 copper ions per protein for spmoB, 1.59 ± 0.84 copper ions per protein for spmoBd1 and 0.24 ± 0.09 copper ions per protein for spmoBd2 (Fig. 2b). These values, which are an average from at least six independent refolding experiments, are consistent with the crystal structure of *M. capsulatus* (Bath) pMMO[6], in which spmoB binds three copper ions and spmoBd2 binds no copper ions. Despite the excess of copper present during the refolding procedure, we do not observe the binding of approximately ten copper ions to spmoBd2 reported previously[16]. Refolding of spmoB in the presence of iron yields 0.17 ± 0.1 iron ions per protein.

The spmoBd1 protein is extremely unstable, probably owing to the removal of spmoBd2. In the *M. capsulatus* (Bath) structure[6], the interface between the two soluble domains is extensive, with a buried

surface area of $\sim 1,400$ Å^2 for each chain. The loop region connecting dicopper ligand His 33 with monocopper ligand His 48 is heavily involved in this interface, with a number of hydrogen bonds (Supplementary Fig. 3a) and hydrophobic contacts with residues from the C-terminal cupredoxin domain. Increased flexibility on disruption of all these interactions probably affects both copper centres and accounts for the reduced copper binding by spmoBd1.

In spite of loading with Cu(II), and possibly owing to photoreduction, the X-ray absorption near-edge spectrum of spmoB (Supplementary Fig. 2) is typical of three- to four-coordinate Cu(I) on the basis of the low intensity of the $1s \rightarrow 4p$ transition, the overall edge structure and the lack of any discernible $1s \rightarrow 3d$ feature. The EXAFS data for spmoB (Fig. 4e, f) were best fitted with a Cu–O/N environment at 1.95 Å and a Cu–Cu interaction at 2.53 Å, the inclusion of which significantly improved the fit (Supplementary Table 2). The combined copper binding and XAS data indicate that spmoB can assemble copper centres similar to those in pMMO.

To determine whether the copper active site is located within spmoB, we performed activity assays. The spmoB protein is indeed active and can oxidize propylene with a specific activity of 30.2 ± 10.5 nmol propylene oxide $\mu mol^{-1} min^{-1}$, as compared with 51.1 ± 11.3 nmol propylene oxide $\mu mol^{-1} min^{-1}$ for as-isolated, membrane-bound pMMO measured under similar experimental conditions (Fig. 5a). Some activity is also detected for spmoBd1, 8.1 ± 3.7 nmol propylene oxide $\mu mol^{-1} min^{-1}$, whereas spmoBd2 is inactive. No activity is detected for spmoB refolded in the presence of iron. Although propylene epoxidation is routinely used for measuring MMO activity, the bond dissociation energies of the C=C bond in propylene (63 kcal mol^{-1}) and the C–H bond in methane (104 kcal mol^{-1}) differ significantly. Therefore, we also tested the ability of spmoB to oxidize methane to methanol. Under similar experimental conditions, the specific activity of as-isolated pMMO is
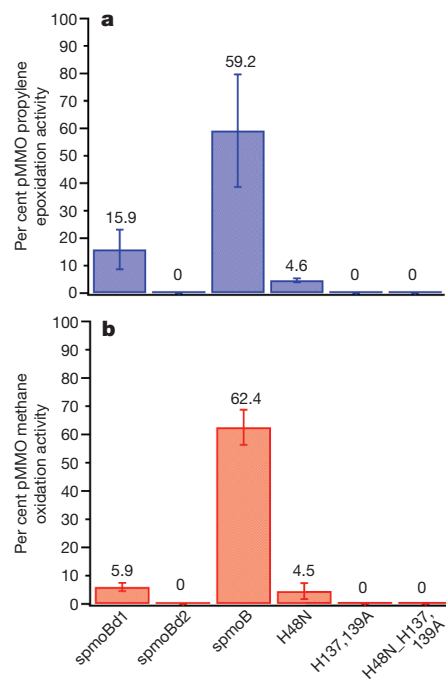

Figure 5 | Catalytic activity of spmoB proteins. a, Epoxidation of propylene to propylene oxide expressed as a percentage of the activity of as-isolated, membrane-bound *M. capsulatus* (Bath) pMMO. **b**, Oxidation of methane to methanol expressed as a percentage of the activity of as-isolated, membrane-bound *M. capsulatus* (Bath) pMMO. All values are the average of at least two independent refolding preparations, with error bars representing standard deviations. The activity of each spmoB protein was compared with the activity of membrane-bound pMMO measured under the same experimental conditions.

325.1 nmol methanol $\mu mol^{-1} min^{-1}$ and that of spmoB is 203.1 ± 20.2 nmol methanol $\mu mol^{-1} min^{-1}$ (Fig. 5b). Consistent with the trend observed for propylene epoxidation activity, spmoBd1 has a specific activity of 19.3 ± 4.7 nmol methanol $\mu mol^{-1} min^{-1}$ and spmoBd2 is inactive. The reduced activity for spmoBd1 is consistent with increased lability of the copper sites on removal of spmoBd2. These combined activity data indicate that the pMMO copper active site is located within spmoB, and rule out the possibility of the active site being a di-iron centre located at the crystallographic zinc site[17] or a trinuclear copper centre located at the intramembrane hydrophilic patch[12]. In addition, the active site is not located in the pmoA subunit as suggested by radio-labelling experiments with the suicide substrate acetylene[24,25].

To pinpoint the active-site location within spmoB, we generated site-specific variants. These variants were designed to disrupt binding at the mononuclear copper site (spmoB_H48N), the dinuclear copper site (spmoB_H137,139A) and both copper sites (spmoB_H48N_H137,139A). Proteins were refolded and the copper content was measured using the same procedures as for spmoB (Fig. 2b). The spmoB_H48N variant (asparagine was selected to mimic the site in *M. trichosporium* OB3b pMMO[10]) binds 1.86 ± 0.52 copper ions per protein, consistent with elimination of the mononuclear site. The spmoB_H137,139A variant binds 0.73 ± 0.15 copper ions per protein, suggesting that the dinuclear copper site has been abolished and the mononuclear copper site remains intact. The spmoB_H48N_H137,139A variant still binds some copper, 0.82 ± 0.36 copper ions per protein, as does a quadruple mutant in which His 33 is changed to alanine. The spmoB_H48N_H137,139A variant refolded in the presence of iron binds 0.51 ± 0.14 iron ions per protein. This metal binding by spmoB_H48N_H137,139A is probably nonspecific and raises the possibility that some fraction of the copper in spmoB_H48N and spmoB_H137,139A is also bound adventitiously.

The copper coordination environments in spmoB_H48N and spmoB_H137,139A were further investigated by X-ray absorption spectroscopy. These two samples contain a mixture of Cu(I) and Cu(II) as shown by both a discernible $1s \rightarrow 4p$ transition and a weak $1s \rightarrow 3d$ feature (Supplementary Fig. 2). The EXAFS data for both variants were best fitted with a Cu–O/N ligand environment at 1.96 Å. For spmoB_H48N, inclusion of a Cu–Cu environment at 2.52 Å improved the fit significantly (Fig. 4g, h and Supplementary Table 2). However, simulations to the second shell for spmoB_H137,139A were improved using carbon as a ligand rather than copper, as suggested by the lower F' value for this fit (Fig. 4i, j and Supplementary Table 2; F' is the number of degrees of freedom weighted degree of deviation between empirical and theoretical spectra). Thus, it is probable that this double mutant does not contain a dinuclear copper centre.

Each variant was then tested for propylene epoxidation and methane oxidation activities (Fig. 5). Only the spmoB_H48N variant was active, with a propylene epoxidation activity of 2.3 ± 0.4 nmol propylene oxide $\mu mol^{-1} min^{-1}$ and a methane oxidation activity of 14.8 ± 9.2 nmol methanol $\mu mol^{-1} min^{-1}$. Because removal of the mononuclear copper site does not abolish activity, it cannot be the active site. By contrast, spmoB_H137,139A and spmoB_H48N_H137,139A show no activity (Fig. 5). These activity results combined with the EXAFS data indicate that the dinuclear copper centre in the pmoB subunit is required for substrate oxidation by pMMO. The dicopper site may not be fully occupied in spmoB_H48N, owing to the presence of adventitious copper, resulting in decreased activity. The activity may be further impaired by the mutation at the monocopper site, which probably imposes some reorganization on the domain interface (Supplementary Fig. 3a). These two considerations could reasonably account for the ~5% activity measured for the spmoB_H48N variant (Fig. 5). The location of the dicopper centre in the pMMO structure (Fig. 1) is consistent with some reduction in activity on isolation of spmoB. A number of pmoB residues adjacent to the dicopper centre interact with residues from the pmoC subunit (Supplementary Fig. 3b).

Removing these interactions probably imparts additional flexibility at the dicopper centre.

Our work shows that pMMO is a copper enzyme and that the active site is located in the N-terminal soluble domain of the pmoB subunit at the site of the crystallographic dicopper centre. Neither the proposed intramembrane di-iron centre[17] nor the proposed intramembrane tricopper centre[12] is the active site. The copper stoichiometry, XAS and activity data are most consistent with a dicopper, rather than a tricopper, active site. Additional support comes from computational studies of methane activation by bis(μ-oxo) dicopper species[26] and reports of direct methane oxidation by mono-(μ-oxo) dicopper cores in zeolites[27]. If spmoB can do the chemistry, it is puzzling why pMMO is a membrane protein. It is possible that substrate entry occurs through the lipid bilayer. The increased solubility of methane in the membrane[28,29] would provide a high local concentration. The methanol product probably exits through the soluble regions because the next metabolic enzyme, methanol dehydrogenase, is periplasmic[30]. The transmembrane regions could also shuttle electrons to the active site and might have other undiscovered activities. Given that the spmoB proteins have less activity than pMMO and that as-isolated pMMO has lower activity than whole cells[17], understanding how the additional subunits and trimeric structure enhance the function is an important issue.

METHODS SUMMARY

We cultivated *M. capsulatus* (Bath) as described previously[9], with minor modifications. Cells were lysed by sonication and ultracentrifuged with multiple washing/homogenization steps to obtain pMMO-containing membranes. Metals were removed from as-isolated pMMO by treatment with KCN. Genes encoding spmoBd1 (residues 33–172), spmoBd2 (residues 265–414) and spmoB (residues 33–172 and residues 265–414 connected by a Gly-Lys-Leu-Gly-Gly-Gly linker instead of the two transmembrane helices) were amplified by PCR and cloned into a pET21b(+) expression vector. We generated site-directed variants using commercial kits. All proteins expressed as inclusion bodies, which were centrifuged and treated with Triton X-100 to obtain >90% pure samples. Purified inclusion bodies were solubilized with urea and refolded by a stepwise dialysis procedure in the presence of CuSO₄. Folding was assessed by circular dichroism spectroscopy and size exclusion chromatography. We determined metal content by the bicinchoninic-acid method[23] or by inductively coupled plasma optical emission spectroscopy. Propylene epoxidation and methane oxidation activities were measured by gas chromatography using Porapak Q packed columns and Rt-Q-BOND capillary columns, respectively. XAS data were collected at the Stanford Synchrotron Radiation Lightsource on beamline 9-3 (ref. 8).

Full Methods and any associated references are available in the online version of the paper at www.nature.com/nature.

1. Hermans, I., Spier, E. S., Neuenschwander, U., Turra, N. & Baiker, A. Selective oxidation catalysis: opportunities and challenges. *Top. Catal.* **52**, 1162–1174 (2009).
2. Arakawa, H. *et al.* Catalysis research of relevance to carbon management: progress, challenges, and opportunities. *Chem. Rev.* **101**, 953–996 (2001).
3. Que, L. & Tolman, W. B. Biologically inspired oxidation catalysis. *Nature* **455**, 333–340 (2008).
4. Merkx, M. *et al.* Dioxygen activation and methane hydroxylation by soluble methane monooxygenase: a tale of two irons and three proteins. *Angew. Chem. Int. Ed.* **40**, 2782–2807 (2001).
5. Hakemian, A. S. & Rosenzweig, A. C. The biochemistry of methane oxidation. *Annu. Rev. Biochem.* **76**, 223–241 (2007).
6. Lieberman, R. L. & Rosenzweig, A. C. Crystal structure of a membrane-bound metalloenzyme that catalyses the biological oxidation of methane. *Nature* **434**, 177–182 (2005).
7. Balasubramanian, R. & Rosenzweig, A. C. Structural and mechanistic insights into methane oxidation by particulate methane monooxygenase. *Acc. Chem. Res.* **40**, 573–580 (2007).
8. Lieberman, R. L. *et al.* Characterization of the particulate methane monooxygenase metal centers in multiple redox states by X-ray absorption spectroscopy. *Inorg. Chem.* **45**, 8372–8381 (2006).
9. Lieberman, R. L. *et al.* Purified particulate methane monooxygenase from *Methylococcus capsulatus* (Bath) is a dimer with both mononuclear copper and a copper-containing cluster. *Proc. Natl Acad. Sci. USA* **100**, 3820–3825 (2003).

10. Hakemian, A. S. *et al.* The metal centers of particulate methane monooxygenase from *Methylosinus trichosporium* OB3b. *Biochemistry* **47**, 6793–6801 (2008).

11. Rosenzweig, A. C. The metal centres of particulate methane monooxygenase. *Biochem. Soc. Trans.* **36**, 1134–1137 (2008).

12. Chan, S. I. & Yu, S. S. F. Controlled oxidation of hydrocarbons by the membrane-bound methane monooxygenase: the case for a tricopper cluster. *Acc. Chem. Res.* **41**, 969–979 (2008).

13. Chen, K. H.-C. *et al.* The copper clusters in the particulate methane monooxygenase (pMMO) from *Methylococcus capsulatus* (Bath). *J. Chin. Chem. Soc.* **51**, 1081–1098 (2004).

14. Nguyen, H.-H. T. *et al.* X-ray absorption and EPR studies on the copper ions associated with the particulate methane monooxygenase from *Methylococcus capsulatus* (Bath). Cu(I) ions and their implications. *J. Am. Chem. Soc.* **118**, 12766–12776 (1996).

15. Chan, S. I. *et al.* Redox potentiometry studies of particulate methane monooxygenase: support for a trinuclear copper cluster active site. *Angew. Chem. Int. Ed.* **46**, 1992–1994 (2007).

16. Yu, S. S.-F. *et al.* The C-terminal aqueous-exposed domain of the 45 kDa subunit of the particulate methane monooxygenase in *Methylococcus capsulatus* (Bath) is a Cu(I) sponge. *Biochemistry* **46**, 13762–13774 (2007).

17. Martinho, M. *et al.* Mössbauer studies of the membrane-associated methane monooxygenase from *Methylococcus capsulatus* Bath: evidence for a diiron center. *J. Am. Chem. Soc.* **129**, 15783–15785 (2007).

18. Choi, D. W. *et al.* The membrane-associated methane monooxygenase pMMO and pMMO-NADH:quinone oxidoreductase complex from *Methylococcus capsulatus* Bath. *J. Bacteriol.* **185**, 5755–5764 (2003).

19. Kitmitto, A., Myronova, N., Basu, P. & Dalton, H. Characterization and structural analysis of an active particulate methane monooxygenase trimer from *Methylococcus capsulatus* (Bath). *Biochemistry* **44**, 10954–10965 (2005).

20. Yu, S. S.-F. *et al.* Production of high-quality particulate methane monooxygenase in high yields from *Methylococcus capsulatus* (Bath) with a hollow-fiber membrane bioreactor. *J. Bacteriol.* **185**, 5915–5924 (2003).

21. Miyaji, A., Suzuki, M., Baba, T., Kamachi, T. & Okura, I. Hydrogen peroxide as an effecter on the inactivation of particulate methane monooxygenase under aerobic conditions. *J. Mol. Catal. B* **57**, 211–215 (2009).

22. Kau, L.-S., Spira-Solomon, D. J., Penner-Hahn, J. E., Hodgson, K. O. & Solomon, E. I. X-ray absorption edge determination of the oxidation state and coordination number of copper. Application to the type 3 site in *Rhus vernicifera* laccase and its reaction with oxygen. *J. Am. Chem. Soc.* **109**, 6433–6442 (1987).

23. Yatsunyk, L. A. & Rosenzweig, A. C. Copper(I) binding and transfer by the N-terminus of the Wilson disease protein. *J. Biol. Chem.* **282**, 8622–8631 (2007).

24. Prior, S. D. & Dalton, H. Acetylene as a suicide substrate and active site probe for methane monooxygenase from *Methylococcus capsulatus* (Bath). *FEMS Microbiol. Lett.* **29**, 105–109 (1985).

25. Zahn, J. A. & DiSpirito, A. A. Membrane-associated methane monooxygenase from *Methylococcus capsulatus* (Bath). *J. Bacteriol.* **178**, 1018–1029 (1996).

26. Shiota, Y. & Yoshizawa, K. Comparison of the reactivity of bis(μ-oxo)Cu^{II}Cu^{III} and Cu^{III}Cu^{III} species to methane. *Inorg. Chem.* **48**, 838–845 (2009).

27. Woertink, J. S. *et al.* A $[Cu_2O]^{2+}$ core in Cu-ZSM-5, the active site in the oxidation of methane to methanol. *Proc. Natl Acad. Sci. USA* **106**, 18908–18913 (2009).

28. Miller, K. W., Hammond, L. & Porter, E. G. The solubility of hydrocarbon gases in lipid bilayers. *Chem. Phys. Lipids* **20**, 229–241 (1977).

29. Batliwala, H., Somasundaram, T., Uzgiris, E. E. & Makowski, L. Methane-induced hemolysis of human erythrocytes. *Biochem. J.* **307**, 433–438 (1995).

30. Myronova, N., Kitmitto, A., Collins, R. F., Miyaji, A. & Dalton, H. Three-dimensional structure determination of a protein supercomplex that oxidizes methane to formaldehyde in *Methylococcus capsulatus* (Bath). *Biochemistry* **45**, 11905–11914 (2006).

Author Contributions R.B., S.M.S., S.R. and L.A.Y. performed experiments. R.B., S.M.S., S.R., T.L.S. and A.C.R. contributed to experimental design, data analysis and manuscript preparation.

Author Information Reprints and permissions information is available at www.nature.com/reprints. The authors declare no competing financial interests. Correspondence and requests for materials should be addressed to T.L.S. (tstemmle@med.wayne.edu) or A.C.R. (amyr@northwestern.edu).

METHODS

Growth of *M. capsulatus* (Bath). *M. capsulatus* (Bath) was cultivated as described previously[9], with a few modifications. Briefly, 12 l of nitrate mineral salts media was supplemented with a trace-element solution, 50 μM $CuSO_4$ and 80 μM FeEDTA. The pH of the culture was maintained at 6.8 using a 100 mM phosphate buffer. Adjustments to the pH during growth were made using NaOH and H_2SO_4. Before growth, methane gas was bubbled through the media for ~30 min. Approximately 5–10 g of highly active cell paste stock was used as the inoculum after resuspension in sterile nitrate mineral salts media at 45 °C. Fermentations were conducted at 45 °C with an air:methane gas ratio of 4:1 and a constant agitation of 300 r.p.m. Cells were harvested at mid-exponential phase ($D_{600 nm}$ = 5–7) and centrifuged for 10 min at 8,000g. Pelleted cells were washed by resuspension in 25 mM PIPES (pH 6.8), re-centrifuged, flash frozen in liquid nitrogen and stored at −80 °C.

Isolation of pMMO-containing membranes. Frozen cells were resuspended in lysis buffer (25 mM PIPES (pH 6.8), 250 mM NaCl) and sonicated on ice. Cell debris was removed by centrifugation at 20,000g for 1.5 h. The lysate was then ultracentrifuged at 160,000g for 1 h to pellet intracytoplasmic membranes. These membranes were resuspended in fresh lysis buffer using a Dounce homogenizer. Ultracentrifugation and resuspension were repeated three times to remove contaminating soluble proteins. SDS–polyacrylamide gel electrophoresis (PAGE) analysis of the as-isolated membranes showed that the predominant component is pMMO. The homogenized crude membranes at ~10–20 mg ml^{-1} were flash frozen in liquid nitrogen and stored at −80 °C.

Preparation of apo-pMMO. Active as-isolated pMMO membranes were incubated with 50 mM MOPS (pH 8.0) and 250 mM NaCl supplemented with a tenfold molar excess (based on copper concentration) of KCN and freshly prepared sodium ascorbate. The addition of ascorbate did not affect the pH of the solution. After a 1-h incubation at room temperature (~25 °C) with stirring, the solution was ultracentrifuged at 160,000g for 30 min to pellet the pMMO membranes. The apo-pMMO membranes were resuspended and washed three times with fresh lysis buffer to remove excess KCN and ascorbate. Cyanide treatment does not alter the integrity of the subunits according to SDS–PAGE. Moreover, apo-pMMO stored at 4 °C has higher activity on copper reactivation than as-isolated pMMO stored at 4 °C for the same time period. This observation suggests that the strict anaerobic protocols used by other researchers[17] might serve to protect against oxidative damage caused by excess metal ions.

Cloning of spmoB, spmoBd1 and spmoBd2. Three constructs of the soluble domain of pmoB (spmoB) were generated: spmoBd1 (residues 33–172), spmoBd2 (residues 265–414) and spmoB (residues 33–172 and residues 265–414 connected by a Gly-Lys-Leu-Gly-Gly-Gly linker rather than by the two transmembrane helices) (Fig. 1). This linker was designed by inspection of the pMMO structure, and the glycine residues were selected to impart flexibility. Primers spmoBd1F (5′-GGA ATT CCA TAT GCA CGG TGA GAA ATC GCA GG-3′) and spmoBd1R (5′-GTG ATC CAA GCT TTC CGG TGG TGA CGG GGT TGC GAA-3′) were used to amplify spmoBd1 from *M. capsulatus* (Bath) genomic DNA. The NdeI–HindIII-digested PCR product encoding spmoBd1 was then ligated into a NdeI–HindIII-digested pET21b(+) vector (Novagen). Primers spmoBd2F (5′-GAG AAG CAA GCT TGG AGG AGG ACA GGC CGC CGG CAC CAT GCG TGG-3′) and spmoBd2R1 (5′-GAG ATC CCA AGC TTA CAT GAA CGA CGG GAT CAG CGG-3′) were used to amplify spmoBd2. The pET21b(+)-spmoBd2 vector was generated by ligation of the PCR product encoding spmoBd2 at the NdeI–HindIII sites. To generate the spmoB construct, HindIII-digested PCR product encoding spmoBd2 amplified using primers spmoBd2F (5′-GAG AAG CAA GCT TGG AGG AGG ACA GGC CGC CGG CAC CAT GCG TGG-3′) and spmoBd2R2 (5′-GAG ATC CCA AGC TTA CAT GAA CGA CGG GAT CAG CGG-3′) was inserted into the HindIII-digested pET21b(+)-spmoBd1 vector. Authenticity of the coding sequences for all constructs was verified by DNA sequencing. There is a silent mutation in the spmoB DNA sequence at position 1,076 that changes C to G (ACC-to-ACG coding for Thr). The site-directed variants spmoB_H48N, spmoB_H137,139A and spmoB_H48N_H137,139A were generated using either a traditional single mutagenesis kit or a multisite-directed mutagenesis kit from Stratagene and verified by DNA sequencing.

Protein expression, purification and refolding. For protein expression, plasmids were transformed into either the BL21(DE3) or the Rosetta (DE3) strain of *E. coli*. Ten millilitres of an overnight culture of freshly transformed cells were transferred to 1 l of LB supplemented with 50 μg ml^{-1} ampicillin. After reaching an attenuation of $D_{600 nm}$ = 0.6 at 37 °C, 0.5 mM IPTG was added and followed by 4 h of post-induction growth. All the expression constructs tested produced proteins that formed inclusion bodies (Supplementary Fig. 4). Alterations to the growth temperature, incubation times, inducer concentrations and growth media had no effect on the protein solubility. Cells from 4 l of growth were

collected by centrifugation at 5,000g for 10 min, washed and resuspended in 200 ml of 20 mM TrisCl (pH 8.0) and 50 mM NaCl, flash frozen in liquid nitrogen and stored at −20 °C until further processed.

Frozen cells were thawed in lukewarm water and lysed by a 10-min sonication cycle of 10 s on/30 s off pulses on ice at 50% output power. Inclusion bodies were separated from cell debris and other soluble proteins by centrifuging for 30 min at 3,000g. The inclusion bodies were then washed three times with 20 mM TrisCl (pH 8.0), 50 mM NaCl and 1.0% Triton X-100, and once more with the same buffer lacking Triton X-100. Inclusion bodies isolated using this procedure were >90% pure and required no additional purification steps (Supplementary Fig. 4). Typically, 1–3 g of inclusion bodies can be isolated from 1 l of cell culture. Purified inclusion bodies were solubilized in 8 M urea (20 ml urea per 1 g). This mixture was left stirring at room temperature for 1 h and then centrifuged at 15,000g for 30 min at room temperature. Urea-solubilized inclusion bodies were aliquoted and stored at –80 °C for further use.

All attempts to express even partly soluble protein were unsuccessful. Therefore, a refolding procedure was developed. Urea-solubilized inclusion bodies were diluted to ~5 mg ml^{-1} protein concentration. Protein refolding was performed using a stepwise dialysis procedure against buffers containing a stepwise reduction in the urea concentration. Each dialysis was performed for at least 3 h. After a 3-h dialysis against 7 M urea, the protein was dialysed against 6 M urea for 3 h and then against 5 M urea for 3 h, and so forth. After dialysis against a buffer containing 0.5 M urea, at least two rounds of dialysis were performed against a buffer containing either 20 mM TrisCl (pH 8.0) or 20 mM PIPES (pH 7.0), and 250 mM NaCl (no urea). On the basis of SDS–PAGE band intensities, we estimate that about 0.2–5% of the total protein was folded after this procedure. Precipitates were removed by centrifugation at 20,000g for 10 min at 4 °C using a tabletop centrifuge. The spmoBd1 variant was generally less stable and more susceptible to precipitation during these procedures.

Circular dichroism spectra were recorded on a JASCO J-715 spectrometer using a 2-mm-path-length quartz cuvette. Proteins were diluted to ~1–2 μM in a buffer of 20 mM potassium phosphate (pH 7.5) and 20 mM potassium fluoride. An average of five scans was collected at 20 °C with 1-nm resolution. Laccase from *Trametes versicolor* (Sigma Aldrich) was used as a model cupredoxin. All the spmoB variants seem folded and have similar secondary-structure properties, suggesting that the mutations do not perturb the overall structure (Supplementary Fig. 5).

Folding was further assessed by analytical size exclusion chromatography on a 21-ml prepacked Superdex G75 column equilibrated with 20 mM PIPES (pH 7.0) and 150 mM NaCl for at least three column volumes. Recombinant proteins were injected in 0.5-ml aliquots and the molecular masses (Supplementary Table 3) were determined using the following standards: blue dextran (void volume), 2 MDa; aldolase, 158 kDa; concanavalin, 75 kDa; albumin, 66 kDa; ovalbumin, 43 kDa; chymotrypsinogen, 25 kDa; RNase, 13.7 kDa; aprotinin, 6.5 kDa. None of the proteins seem to form trimers, suggesting that the transmembrane regions of pMMO drive oligomerization.

Copper loading of recombinant proteins. The spmoB protein contains the ligands to the two copper sites observed in the *M. capsulatus* (Bath) crystal structure (Fig. 1). Complete precipitation occurred on copper addition to refolded spmoB. Therefore, a refolding procedure in the presence of copper was developed and used for all spmoB variants. The 6 M urea dialysis buffer included 1 mM $CuSO_4$, and the stepwise reduction in urea concentration was accompanied by a reduction in copper concentration. Excess copper was then removed from Cu(II)-refolded proteins by dialysis against a buffer containing either 20 mM TrisCl (pH 8.0) or 20 mM PIPES (pH 7.0), and 250 mM NaCl, with no $CuSO_4$ or urea. Proteins refolded following this procedure contained no detectable iron. For refolding of spmoB and its variants in the presence of iron, 1 mM $Fe(NH_4)_2(SO_4)_2$ was added during dialysis instead of $CuSO_4$. All other procedures were identical to those used for refolding in the presence of copper.

Determination of metal content. The copper contents of spmoB variants were measured using the bicinchoninic-acid (BCA) method[23]. Standards of 0–60 μM copper were prepared by diluting commercially available copper atomic absorption spectroscopy standard solutions (Sigma Aldrich) in water. The Cu(I)–BCA complex has absorbance peaks at 360 and 562 nm. The iron contents of spmoB variants were determined using the ferrozine assay[31]. A solution containing 150 μl 1 M HCl, 150 μl freshly prepared 1.7 mM ascorbate and 250 μl 0.1% ferrozine (Acros Organics) prepared in 50% ammonium acetate was added to 150 μl protein. The reaction mixture was incubated at 30 °C for 15 min, centrifuged and the absorbance at 570 nm of the supernatant measured. A standard curve using iron atomic absorption standard (Aldrich) was generated for a 0–40 μM iron concentration range. The copper, iron and zinc contents of as-isolated pMMO membranes and apo-pMMO membranes were determined by inductively coupled plasma optical emission spectroscopy (ICP–OES) using a

Varian Vista-MPX charge-coupled-device simultaneous ICP–OES instrument in the Integrated Molecular Structure Education and Research Center at Northwestern University. Samples were digested in 5% trace-metal grade (TMG) nitric acid before analysis. Standard curves were generated from atomic absorption standards diluted in 5% nitric acid (TMG). All samples were measured in triplicate. Protein concentrations were determined using either Bradford reagent or detergent-compatible Bio-Rad D_c protein assays. Alternatively, estimated extinction coefficients for the absorbance at 280 nm were used for the spmoB variants.

Propylene epoxidation assay. pMMO activity was assessed by the propylene epoxidation assay using duroquinol as the reductant[9]. In a typical assay, solid duroquinol is added to 50 μl as-isolated pMMO in a septa-sealed 3-ml reaction vial such that the final concentration of duroquinol is 0.9–1.1 M. The assay is then initiated by replacing 2 ml of the headspace gas with propylene and the vial is shaken in a 45 °C water bath for 3 min. The amount of propylene oxide produced is measured by injecting 250 μl of headspace gas onto a Porapak Q column (Supelco) using a Hewlett Packard 5890A gas chromatograph. Quantitation is performed by comparison with pure propylene oxide standards (Sigma Aldrich). Typical activity values were between 50–200 nmol propylene oxide mg^{-1} min^{-1} (Supplementary Table 1). For metal-reconstituted-activity assays, apo-pMMO was incubated with varying molar equivalents of CuSO$_4$ and/or Fe(NH$_4$)$_2$(SO$_4$)$_2$ for 30 min and measurements performed as above. The CuSO$_4$ solution (280 p.p.m.) contained <0.02 p.p.m. iron, so addition of 1 equiv. of copper would correspond to ~10^{-7} equiv. of iron. The iron content of apo-pMMO reconstituted with copper did not increase. The titration results shown in Fig. 3 were reproduced more than four times. For experiments with catalase, commercial enzyme (Sigma Aldrich) was added at a concentration of ~1 mg ml^{-1} to samples reconstituted with more than 2–3 equiv. of copper (Supplementary Fig. 1b).

For the spmoB variants, the propylene epoxidation assay was performed with several modifications. Briefly, protein sample volumes were 350 μl and headspace air (2.5 ml) was replaced with 2.0 ml propylene and 0.5 ml air. The reaction mixture was incubated in the 45 °C shaking water bath for at least 1 h. A longer incubation time for spmoB was required to accurately measure product formation. For comparisons of the spmoB activity with that of as-isolated pMMO, the pMMO assay was also carried out for 1 h (Fig. 5). All activity assays were performed in duplicate. To account for the differences in molecular masses when comparing activities of pMMO (~100 kDa) with those of spmoB and its variants (~16–32 kDa), the activities of spmoB and its variants are reported per mole instead of per milligram.

Methane oxidation assay. Methanol production by both pMMO and the spmoB variants was measured by gas chromatography using a Rt-Q-BOND capillary column (Restek). The procedure for the propylene epoxidation assay was used with the following modifications. Methane (2 ml) was added to the headspace instead of propylene as the substrate. The reaction was performed for 3 min at 45 °C for pMMO (Fig. 3) and for at least 1 h at 45 °C for spmoB and its variants (Fig. 5). For comparisons of the spmoB activity with that of as-isolated pMMO, the pMMO assay was also carried out for 1 h (Fig. 5). After this procedure, the samples were heated to 85 °C for 10 min to stop the reaction, and cooled on ice. Samples were then centrifuged briefly and 3 μl of the clear supernatant injected onto the capillary column at a constant oven temperature of 75 °C. Quantitation was performed using standard curves generated by analysing methanol standards (Sigma Aldrich; spectrophotometric grade >99%). For both propylene epoxidation and methane oxidation assays, numerous control assays in which duroquinol, substrate or enzyme was eliminated systematically from the reaction mixture were performed.

X-ray absorption spectroscopy. XAS data were collected on the following five samples: as-isolated pMMO (sample 1), apo-pMMO reconstituted with CuSO$_4$ in the presence of duroquinol (sample 2), spmoB (sample 3), spmoB_H48N (sample 4) and spmoB_H137,139A (sample 5). As-isolated and apo-pMMO membranes were ultracentrifuged and resuspended in 25 mM PIPES (pH 6.8), 250 mM NaCl and 50% glycerol before loading into Kapton-tape-wrapped Lucite cells and flash freezing in liquid nitrogen. The samples were stored in liquid nitrogen until data collection was performed. For reconstituted pMMO membranes, apo samples were incubated with 3 equiv. of CuSO$_4$ for 30 min; this was followed by addition of excess duroquinol, ultracentrifugation, resuspension, cell loading and freezing. The final copper concentrations were 0.7–2 mM. For spmoB and its variants, all samples were prepared in 10 mM TrisCl (pH 8.0), 250 mM NaCl and 50% glycerol. The final copper concentrations were 0.3–0.9 mM. All XAS results were reproduced using two independent samples.

XAS data were collected at the SSRL on beamline 9-3 using a Si(220) double-crystal monochromator equipped with a harmonic rejection mirror. Samples were maintained at 10 K using an Oxford Instruments continuous-flow liquid helium cryostat. Protein fluorescence excitation spectra were collected using a 30-element germanium solid-state array detector. A nickel filter (0.3 μm wide) was placed between the cryostat and the detector to filter scattering fluorescence not associated with protein copper signals. XAS spectra were measured using 5-eV steps in the pre-edge region (8,750–8,960 eV), 0.25-eV steps in the edge region (8,986–9,050 eV) and 0.05 Å^{-1} increments in the EXAFS region (to k = 13.0 Å^{-1}), integrating from 1 s to 20 s in a k^3-weighted manner for a total scan length of approximately 45 min. X-ray energies within the protein spectra were internally calibrated by simultaneously collecting copper foil absorption spectra; the first inflection point in the copper foil spectra was assigned as 8,980 eV. Each fluorescence channel of each scan was examined for spectral anomalies before averaging, and spectra were closely monitored for photoreduction. The represented data are the average of seven or eight scans.

XAS data were processed using the Macintosh OS X version of the EXAFSPAK program suite[32] integrated with the FEFF 7 software[33] for theoretical model generation. Data reduction followed a previously published protocol for a spectral resolution in bond lengths of 0.13 Å (ref. 8). EXAFS fitting analysis was performed on raw/unfiltered data. Protein EXAFS data were fitted either using single-scattering FEFF 7 theoretical models, calculated for carbon, oxygen, sulphur and copper coordination to simulate copper-ligand environments, or a multiple-scattering imidazole model, and values for the scale factors (Sc) and E_o calibrated by fitting crystallographically characterized copper model compounds, as outlined previously[8]. Criteria for judging the best-fit EXAFS simulations used both the lowest mean square deviation between data and fit corrected for the number of degrees of freedom (F')[34] and reasonable Debye–Waller factors ($\sigma^2 < 0.006$ Å^2). First-shell fits with a single set of O/N ligands gave significantly better F' values than fits with a single Cu–S or Cu–Cu environment for all samples. Long-range scattering (>3 Å) evident for all five samples could not be fitted with a multiple-scattering Cu-imidazole model, as shown by the large F' values for these fits (Supplementary Table 2, fits 1.3, 2.3, 3.3, 4.3 and 5.3).

31. Stookey, L. L. Ferrozine - a new spectrophotometric reagent for iron. *Anal. Chem.* **42,** 779–781 (1970).
32. George, G. N., George, S. J. & Pickering, I. J. *EXAFSPAK* ⟨http://www-ssrl.slac.stanford.edu/~george/exafspak/exafs.htm⟩ (2001).
33. Ankudinov, A. L. & Rehr, J. J. Relativistic calculations of spin-dependent X-ray absorption spectra. *Phys. Rev. B* **56,** R1712–R1716 (1997).
34. Riggs-Gelasco, P. J., Stemmler, T. L. & Penner-Hahn, J. E. XAFS of dinuclear metal sites in proteins and model compounds. *Coord. Chem. Rev.* **144,** 245–286 (1995).